Flight Mission Feasibility Assessment of Urban Air Mobility Operations under Battery Energy Constraint

Abenezer G. Taye*
George Washington University, Washington, DC, 20052, USA

Peng Wei†
George Washington University, Washington, DC, 20052, USA

This paper introduces a decision-making framework for Urban Air Mobility (UAM) and Unmanned Aerial Systems (UAS) operations that addresses the dual challenges of collision safety and battery energy constraints. To address these issues, the paper proposes a novel two-layer algorithmic framework that conducts pre-departure flight planning and flight mission risk assessment in relation to available battery energy. The upper layer is responsible for strategic de-confliction, while the lower layer performs prognostics and decision-making regarding the execution of the mission. The efficacy of this framework is demonstrated in a UAS scenario designed for package delivery in the University Park area of the Dallas-Fort Worth metropolitan region. The results highlight the framework's potential to enhance safety and energy efficiency in UAM and UAS operations.

I. Introduction

Urban Air Mobility (UAM) is a novel concept in which partially or fully autonomous air vehicles transport passengers and cargo in dense urban environments. This innovative technology aims to offer a safe, efficient, and accessible alternative to traditional ground-based transportation methods. As it advances, UAM is expected to connect urban centers with outlying areas, thereby expanding the reach of metropolitan regions [1].

The development of UAM is projected to evolve from initial low-density, simple operations to an advanced stage of highly automated, dense, and complex on-demand services [2]. These services will likely involve hundreds to thousands of simultaneous urban airspace operations. To achieve this, the development and use of automated tools, known as providers of services (PSU), are crucial. These tools aid in the planning and decision-making process, with a primary focus on ensuring the safe operation of aircraft in this safety-critical application.

This paper specifically addresses two major factors that influence the safety performance of UAM operations: the potential for collisions between aircraft and the challenges posed by insufficient battery energy. In the context of UAM, strategic de-confliction is envisioned to manage separation assurance and collision avoidance [3], where part of the

*Graduate Student, Department of Mechanical & Aerospace Engineering, abenezertaye@gwu.edu, AIAA Student Member.
†Associate Professor, Department of Mechanical & Aerospace Engineering, pwei@gwu.edu, AIAA Associate Fellow.

airspace is reserved for an aircraft before its departure, ensuring that no other aircraft can use it simultaneously.

On the other hand, given that UAM is expected to rely on electric-powered aircraft, commonly referred to as eVTOLs (electric vertical takeoff and landing aircraft), the feasibility of strategically de-conflicted flight plans could be compromised by insufficient battery energy. To address this, the paper presents an automated tool that performs pre-departure flight planning and flight mission risk assessment, considering available battery energy.

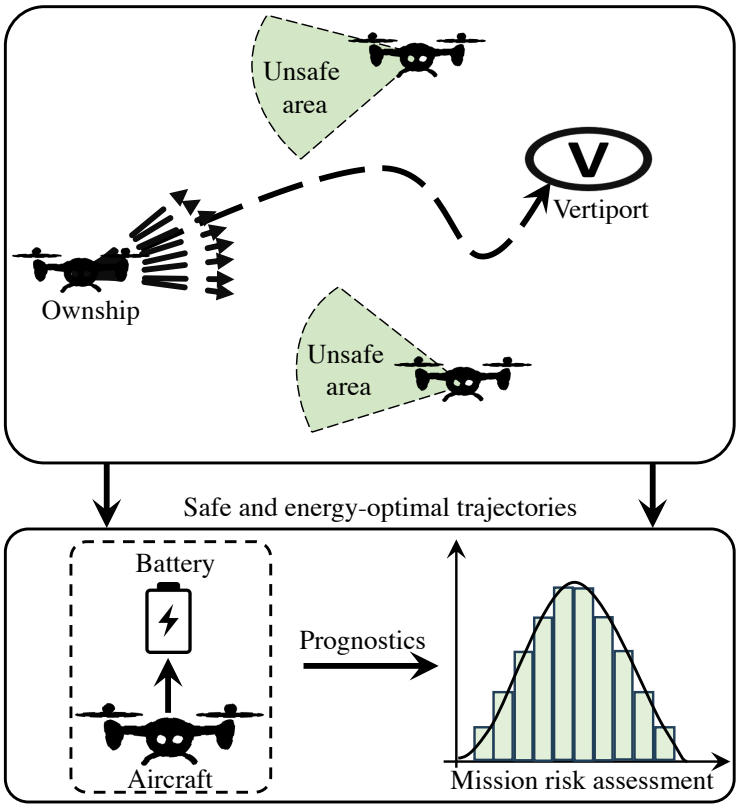

Fig. 1 Working principle of the proposed framework.

Therefore, the overall objective of this paper is to introduce a decision-making framework that facilitates the generation of energy-optimal and strategically de-conflicted flight plans, as well as the assessment of risks associated with insufficient battery energy. To address this challenge, we present a comprehensive algorithmic framework, illustrated in Figure 1, which employs a two-layer approach. The upper layer is responsible for safe and energy-optimal trajectory planning, while the lower layer handles prognostics and decision-making regarding the execution of the mission. It is important to note that while this framework is applicable to any electric-powered aerial transportation, including larger eVTOLs used for passenger transport in UAM, the focus of this paper is on a smaller unmanned aerial system (UAS) for package delivery purposes, with a scenario implemented in the Dallas-Fort Worth (DFW) area.

II. Related Work

In this study, we adopted unstructured airspace topology with free-flight concept of operation. Free flight concept of operation has several advantages such as the ability to handle higher traffic density, as demonstrated in [4], and the potential for fuel and time efficiency, as noted in [5, 6]. As a result, it is becoming increasingly prefered for UAM applications [7].

The current body of literature exploring the feasibility of the free-flight operation concept is limited; nevertheless, some prior works have addressed this issue in different contexts. Among these, Paielli, *et. al.* [8] discussed the problem of estimating the conflict probability for aircraft, taking into account the uncertainty associated with the aircraft's trajectory and speed. Bowers, *et. al.* [9] proposed a method for assessing the feasibility of a proposed flight profile based on several constraints, such as aircraft performance, airspace and traffic flow, and weather-related constraints. Wing, *et. al.* [10] proposed a pilot-in-command (PIC) model for autonomous flight operations and evaluated the feasibility of the concept by considering issues such as safety, security, and operational efficiency.

From a battery energy-related flight planning perspective, several previous studies have explored the impacts of battery energy on the operational decision-making of autonomous flight systems. Corbetta *et al.* [11] presented a framework to quantify uncertainty in mission success due to available battery energy, but only considered the power train model of a UAV. Quinones-Grueiro *et al.* [12] studied the UAV navigation problem in urban environments while taking the battery energy into account. Pradeep *et al.* [13] used an optimal control framework for a multi-rotor eVTOL aircraft to achieve energy-efficient arrival with a required time of arrival constraint, and [14] proposed an approach to generate wind-optimal trajectories for UAM missions with minimum energy consumption. Additionally, Schumann *et al.* [15] introduced a prognostics-as-a-service (PaaS) framework for UAVs that monitors the health and state of charge of the battery (SoC), among other features of the UAV online, communicates the state of the aircraft to ground controllers, and can perform contingency planning. Furthermore, in [16], we considered complex aircraft and battery dynamic models, along with actual wind forecasts, to examine the impact of battery energy on flight missions. However, none of these studies addressed the coupled problem of multi-agent strategic de-confliction and the feasibility of each flight mission with respect to the available battery energy before the aircraft takes off.

Therefore, the two key contributions of the paper are:

- We proposed a pre-departure flight planning framework that generates safe and energy-optimal trajectories.
- We proposed a prognostics-based pre-departure decision-making framework that takes into account the available battery energy and decides whether to execute the mission.

III. Modeling and Solution Methods

The two major tasks of the proposed framework are pre-departure flight planning and mission risk assessment with respect to battery energy. These tasks are carried out by the two layers of the framework: the lower layer and the upper

layer. The upper layer is tasked with generating safe and energy-optimal trajectories for each agent in the environment, guiding the aircraft from its starting point to its final destination, i.e., strategic de-confliction. On the other hand, the lower layer takes the trajectories from the upper layer and applies a model-based prognostics architecture to compute the risk of mission success and determine the feasibility of the mission. This section discusses the formulation of these two layers.

A. Upper Layer: Trajectory Planner

The trajectory planner implemented in this paper, introduced in [7] and [17], represents the decision-making problem as a Markov decision process (MDP). An MDP is defined as a tuple (s_t, a_t, r_t, t), where $s_t \in S$ is the state at time t, $a_t \in A$ is the action chosen by the agent at time t as a result of the decision process, and r_t is the reward received by the agent for executing a_t from s_t and reaching s_{t+1}. The transition function $T(s_t, a, s_{t+1})$ is used to describe the dynamics of the environment. The solution to MDP, the optimal policy π^*, specifies the optimal action $a^* \in A$ to take from each state $s \in S$ to maximize the expected return. The maximum expected value obtained from each state $s \in S$ is represented by the optimal value function $V^*(s)$, computed from π^*, with π^* also being recoverable from $V^*(s)$.

A significant update to the current planner, as compared to [17], is the inclusion of energy considerations in the trajectory planning problem. Therefore, this paper focuses on highlighting the main components of the planner, with a particular emphasis on the energy-related reward function. It is also worth noting that, although the trajectory planner is designed for online guidance of aircraft in a free-flight manner, in this study, it has been employed offline to perform pre-departure flight planning and strategic de-confliction.

1. State Space

The environment is a continuous state space placed on a rectangular area of **7 km^2**. Given the dynamics of an aircraft:

$$\dot{\zeta}(t) = f(\zeta(t), u(t)), \tag{1}$$

where, $f : \mathbb{R}^n \times \mathbb{R} \rightarrow \mathbb{R}^n$ is a continuous function. ζ denotes the aircraft states. The trajectory of an aircraft $\xi : \mathbb{R}^n \times \mathbb{R}_{\geq 0} \rightarrow \mathbb{R}^n$ is the solution to the differential equation (1). For a given initial set $x_0 \in \mathbb{R}^n$, the state of the system at time t is $\xi(\zeta_0, t) = \zeta(t)$. The control input $u(t)$ is comprised of the thrust T, and the three torques τ_θ, τ_ψ, and τ_ψ. In addition, a single state in the state space (s_o) contains all the states of an aircraft (ζ) and the states of every other aircraft denoted as $f_j, \forall j \in J$. Thus, we can define s_o as $s_o = [\zeta, f_1, ..., f_j]$, where j represents the number of other aircraft.

2. Aircraft Dynamics

The state transition function $T(s_t, a, s_{t+1})$ of the MDP-based decision maker is given by a 6-DOF low-fidelity dynamic model of octo-rotors, adopted from [18], where inertia is described by lumped masses. The model employs lumped masses to describe the inertia and provides a balance between accuracy and computational efficiency. As such, it accurately represents the behavior of the aircraft without imposing excessive computational load. The model is formulated in the state-space representation as shown in Equation 2, where s, c, and t denote sin, cos, and tan functions, respectively.

$$\dot{x} = \begin{bmatrix} \dot{x} \\ \dot{y} \\ \dot{z} \\ (s_\theta c_\psi c_\phi + s_\phi s_\psi)\frac{T}{m_t} \\ (s_\theta s_\psi c_\phi - s_\phi s_\psi)\frac{T}{m_t} \\ -g + c_\phi c_\theta \frac{T}{m_t} \\ p + q s_\phi t_\theta + r c_\phi t_\theta \\ q c_\phi - r s_\phi \\ q\frac{s_\phi}{c\theta} + r\frac{c_\phi}{c\theta} \\ \frac{I_{ybyb} - I_{zbzb}}{I_{xbxb}} qr + \frac{l}{I_{xbxb}}\tau_\phi \\ \frac{I_{zbzb} - I_{xbxb}}{I_{ybyb}} pr + \frac{l}{I_{ybyb}}\tau_\theta \\ \frac{I_{xbxb} - I_{ybyb}}{I_{zbzb}} pr + \frac{l}{I_{zbzb}}\tau_\psi \end{bmatrix} \tag{2}$$

In the above equation, linear position and velocity variables are represented by $s, \dot{s}$, and angular position and velocity variables by $[\phi, \theta, \psi]$ and $[p, q, r]$, respectively. The state vector is defined as $x = [s, \dot{s}, \phi, \theta, \psi, p, q, r]^T$. Additionally, g denotes the gravitational constant, m_t represents the lumped mass, and l is the arm length.

3. Action Space

The action space of the MDP is composed of the individual action spaces of the four inputs: the thrust T, and three torques τ_θ, τ_ψ, and τ_ϕ. The action space of T is composed of 10 linearly spaced discrete values between $0Nm$ and $200Nm$. The chosen minimum and maximum values are determined by the performance capabilities of the motors (KDE-4213XF motors) in terms of the delivered thrust and torque. Consequently, the inputs of τ_θ, τ_ψ, and τ_ϕ are logarithmically spaced within a range of 10 input values.

The logarithmically spaced input set in degree/second is computed as follows:

$$\tau_\theta = [-100.00, -31.62, -10.00, -3.16, -1.00, 10.00, 17.78, 31.62, 56.23, 100.00] \tag{3}$$

$$\tau_\psi = [-100.00, -31.62, -10.00, -3.16, -1.00, 10.00, 17.78, 31.62, 56.23, 100.00] \tag{4}$$

$$\tau_\phi = [-100.00, -31.62, -10.00, -3.16, -1.00, 10.00, 17.78, 31.62, 56.23, 100.00] \tag{5}$$

Finally, the joint action space becomes:

$$\mathcal{A} = \{T, \tau_\theta, \tau_\psi, \tau_\psi\}. \tag{6}$$

4. Reward Function

The reward function is the primary mechanism to control the behavior of an MDP agent. It is defined as $R(s_t, a_t, s_{t+1})$, representing the reward an agent collects when it transitions from state s_t to s_{t+1} after taking action a_t. In this work, we have utilized both positive and negative rewards, as depicted in Table 1, to guide the aircraft to their destination while avoiding potential collision with nearby aircraft. Additionally, negative rewards have been introduced to reduce maneuvers that result in high energy consumption.

The type of trajectory generated and the maneuvers required to execute it are crucial in determining the feasibility of a flight mission concerning the available battery energy. This necessitates the generation of an energy-optimal trajectory, a concept often referred to as trajectory optimization in the literature [19]. To achieve this, our reward function penalizes the trajectory planning agent for generating trajectories that demand excessive energy. Since the trajectory planner inherently operates as a finite horizon decision-making framework, penalizing changes in aircraft positions $(\Delta x, \Delta y, \Delta z)$ that lead to high energy consumption is an effective strategy.

To this end, we trained the following regression model that predicts energy consumption based on changes in aircraft positions.

$$\mathbf{E}_{\text{cons}} = \mathbf{A}^\top \cdot \Delta\mathbf{d} + \mathbf{B}^\top \tag{7}$$

where $\mathbf{A}^\top$ and $\mathbf{B}^\top$ are the transposed coefficient vectors of the energy consumption model, they are defined as follows:

$$\mathbf{A} = [0, 520.699, 203.742, 127.606, 86.3024, 71.8159, 63.1053, 57.9294, 50.7294, 46.399],$$
$$\mathbf{B} = [0, 369.168, 869.01, 1119.61, 1459.52, 1368.97, 1279.89, 1128.54, 1144.29, 1183.82].$$

In addition, the vector $\Delta\mathbf{d} = [\Delta d_1, \Delta d_2, \ldots, \Delta d_n]$ represents the change in distance traveled by the aircraft from its

current position to the n^{th} future state and can be mathematically described as:

$$\Delta d_n = \sum_{i=1}^{n} \sqrt{(x_i - x_{i-1})^2 + (y_i - y_{i-1})^2 + (z_i - z_{i-1})^2} \tag{8}$$

This regression model, multiplied by a constant factor κ, serves as a reward function to penalize the trajectory planning agent when it attempts to generate a trajectory that leads to high energy consumption.

Table 1 Reward Functions for Each Aircraft

Reward Source	Reward Magnitude	Location	Decay Factor	Purpose
Intruder aircraft	$-(100t + 500)$	Intruder	0.97	Collision avoidance
Destination	200	Manually placed	0.999	Vertiport attraction
Energy consumption	$\kappa(\mathbf{A}^\top \cdot \Delta\mathbf{d} + \mathbf{B}^\top)$	Aircraft next states	0	Minimize energy consumption

The trajectory planner first assigns the initial and goal states for each aircraft in the system. Then, for each aircraft, it identifies the positive and negative reward sources as discussed in III.A.4. Once the reward sources are identified, it forward projects the future states of the aircraft using the action sets and computes the values of each future state using the value function. Then, it picks the best action that yields the maximum total reward and updates the states of the aircraft using the selected control action. This procedure will be carried out for each aircraft iteratively until each aircraft reaches its destination vertiport.

B. Lower Layer: Battery Prognostics and Decision Making

A key task in assessing the risk of a mission related to battery energy is predicting the battery's state of charge (SoC) at the end of the flight mission. The SoC of a battery is typically defined as 1 when the battery is fully charged and 0 when it is discharged to a predetermined voltage threshold. Such a task is known as prognostics, and we adopted model-based prognostics architecture from [20] and its implementation from [21]. The architecture is summarized as follows:

Given a system model defined as:

$$x(k+1) = f(k, x(k), \theta(k), u(k), v(k)), \tag{9}$$

$$y(k) = h(k, x(k), \theta, u(k), n(k)), \tag{10}$$

where k is the discrete time variable, $x(k) \in R^{n_x}$ is the sate vector, $\theta(k) \in R^{n_\theta}$ is unknown parameter vector, $u(k) \in R^{n_u}$ is the input vector, $v(k) \in R^{n_v}$ is the process noise vector, f is the state equation, $y(k) \in R^{n_y}$ is the output vector, $n(k) \in R^{n_n}$ is the measurement noise vector, and h is the output model.

The battery model utilized in this study is an electrochemical-based model of Lithium-ion batteries, as described in

[20], which are a popular choice for powering unmanned aerial vehicles. In this model, the battery's current draw (I) serves as the input, while the battery temperature (tb) and the voltage drop caused by solid-phase ohmic resistance (V_o) represent its outputs ($y(k)$).

The prognostics architecture comprises two major steps: estimation and prediction. the joint state-parameter estimate $p(x(k), \theta(k)|y(k_0 : k))$ is computed using the system dynamics and observation history up to time k represented as $y(k_0 : k)$. On the other hand, in the prediction step, the probability distribution $p(k_E(k_P)|y(k_0 : k_P))$ at prediction time k_p is computed using the joint state-parameter estimate and hypothesized future inputs of the system. The estimation algorithm used in this paper is the Unscented Kalman Filter (UKF) [22], along with the battery model. The UKF uses sigma points which are deterministic points that are used to represent the joint state-parameter distribution $p(x(k), \theta(k), |y(k_0 : k))$. The predictor algorithm used in this paper is the Monte Carlo predictor [23], which randomly samples from the battery's current state distribution, and each sample is simulated to the end of the flight. By collecting a set of SoC values from several Monte Carlo simulations, the probability distribution can be built, and the probability of mission success at a given time t can be computed using the following equation:

$$P_{\text{success}}(t) = \frac{\sum_{i=1}^{n}(\text{SoC}_i(t) > \text{SoC}_{\text{th}})}{n} \tag{11}$$

where n represents the number of Monte Carlo simulations in the prediction step and SoC_{th} is the threshold battery SoC value required at the end of flight.

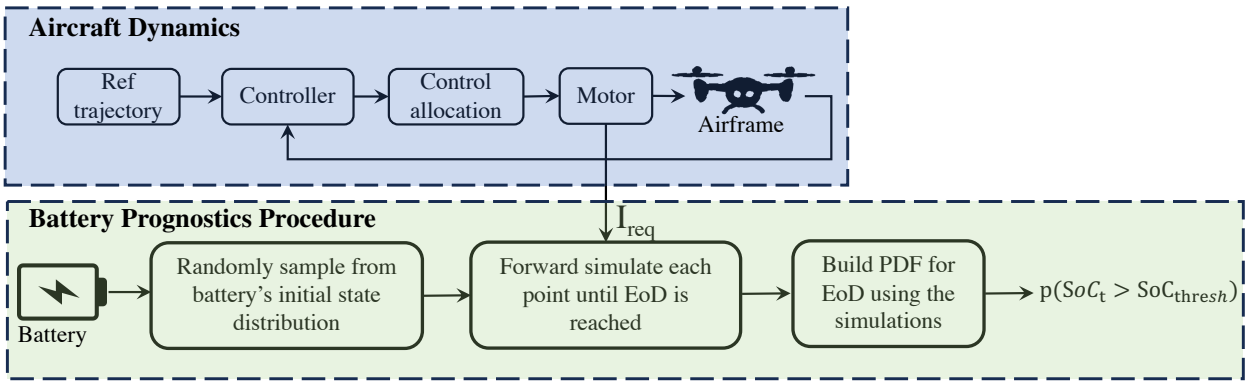

Fig. 2 Schematic diagram representation of the battery's SoC prediction procedure

The battery SoC prediction process is illustrated in Figure 2. According to the procedure, given a reference trajectory and information about the available battery energy, the first step is to simulate the high-fidelity octo-rotor model adopted from [24] along the trajectory to obtain the mission's current requirement (I_{req}), which is used as a future load for battery SoC prediction. Once the mission's I_{req} is known, the battery model will be simulated from its initial state until SoC is reached. Finally, the predicted SoC points are collected, and the probability density function for battery SoC at

the flight end time is constructed.

C. Overall Framework

The overall working procedure of the framework is presented in Algorithm 1. The inputs to the framework are the aircraft's initial state and destination, the battery's initial state (x_0), and mission success probability threshold $P_{\text{threshold}}$ to determine whether to conduct the mission or not. The framework's output is the decision to either take off or hold the aircraft. The first step is generating trajectories from start to destination for each aircraft. These trajectories are safe (in terms of collision avoidance with other aircraft) and locally energy optimal. Next, before proceeding to the battery prognostics process, we sample waypoints from the generated trajectories and feed those waypoints to the detailed aircraft dynamics as a reference trajectory. Then, we run the detailed octo-rotor dynamics and collect the current requirements of the missions. Once the current requirement is collected, we randomly sample from the battery's initial state and simulate the battery model until the end of the flight is reached.

Algorithm 1: Pre-departure Flight Planning and Mission Risk Assessment Framework

Procedure `FlightPlanAndRiskAssessment()`:
- **Input :** Aircraft initial state and destination, Battery initial state (x_0) and $P_{\text{threshold}}$
- **Output :** Decision to either take off or hold the aircraft

1 **for** *each aircraft i* **do**
2 Generate safe and energy optimal trajectory from start to destination
3 Obtain the current requirement of the trajectory
4 Perform Monte Carlo (MC) simulations of the battery using the current requirement
5 Construct End-of-Flight Battery SoC Probability Density Function (PDF) from MC simulation results
6 Compute the probability of mission success using Equation 11
7 **if** $P_{success} > P_{threshold}$ **then**
Execute the mission
8 **else**
Keep charging the aircraft and/or re-plan the flight trajectory
9 End of operation

IV. Simulation and Results

A. Scenario Description

The scenario we used to implement the framework and test its performance is shown in Figure 4. This scenario, designed for a package delivery application, is implemented for the University Park area of Dallas-Fort Worth metropolitan region. It includes three depots from which aircraft are expected to take off, and random destination places can be assigned within the **7 km^2** rectangular area.

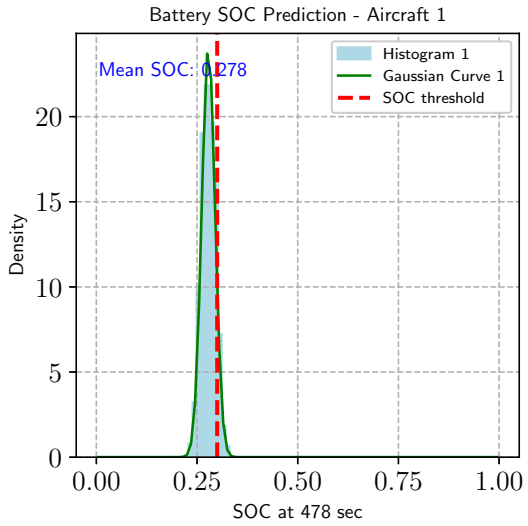

(a) SoC Prediction for Aircraft 1

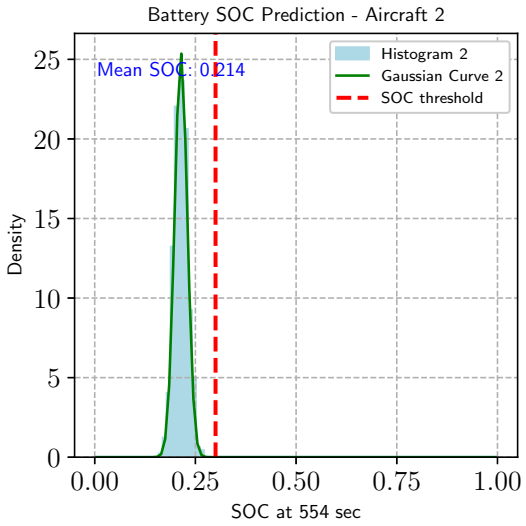

(b) SoC Prediction for Aircraft 2

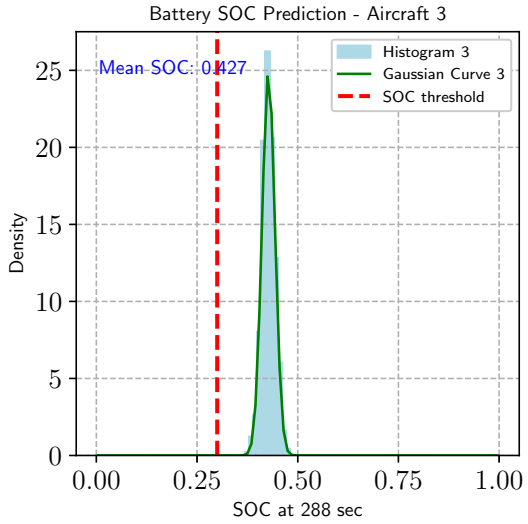

(c) SoC Prediction for Aircraft 3

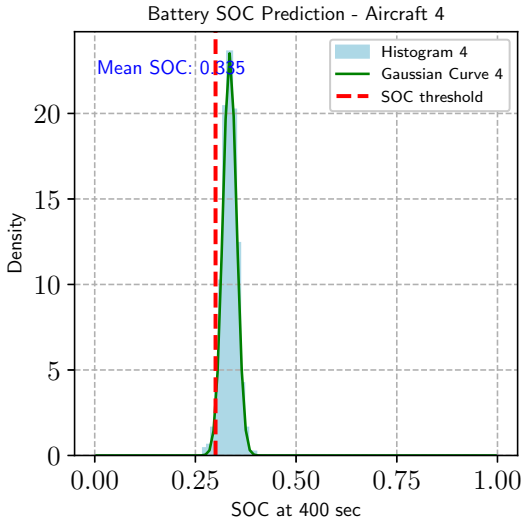

(d) SoC Prediction for Aircraft 4

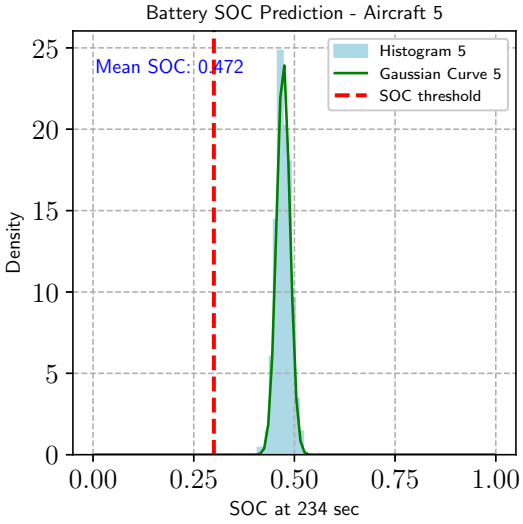

(e) SoC Prediction for Aircraft 5

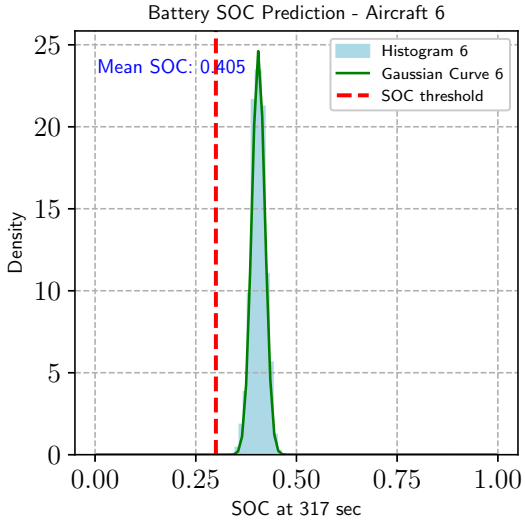

(f) SoC Prediction for Aircraft 6

Fig. 3 Battery SOC predictions for all aircraft

B. Results

Although the environment can accommodate a configurable number of aircraft that use the proposed decision-making framework, we present experimental results for a specific case involving six aircraft. These aircraft are assigned to take off from three depots and fly to six different destinations. The safe and energy-optimal trajectories generated by the upper layer of the framework are visualized in Figure 4. In the figure, the red rectangle depicts the rectangular area considered within the DFW region for the package delivery scenario. Additionally, the strategically de-conflicted trajectories for each aircraft, from their assigned depots to their destinations, are plotted in various colors.

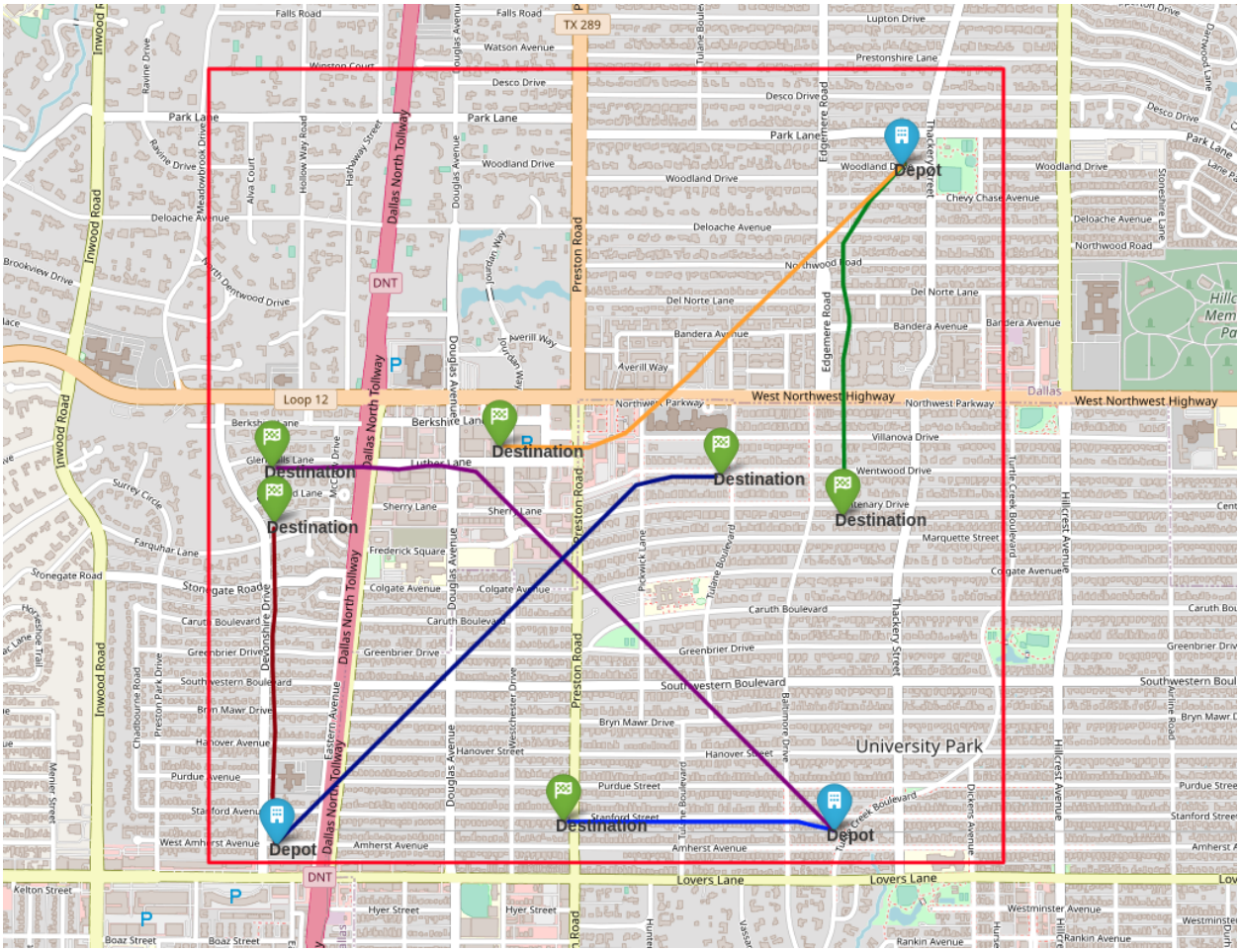

Fig. 4 The drone package delivery scenario implemented in the University Park area of the Dallas-Fort Worth metropolitan region

Moreover, the effect of the energy-related reward function discussed in Section III.A.4, on the overall power consumption and cumulative energy of an aircraft is depicted in Figure 5. As illustrated in the figure, the trajectory generated by the planner, which incorporates the energy-related reward function, shows a significant reduction in cumulative energy consumption.

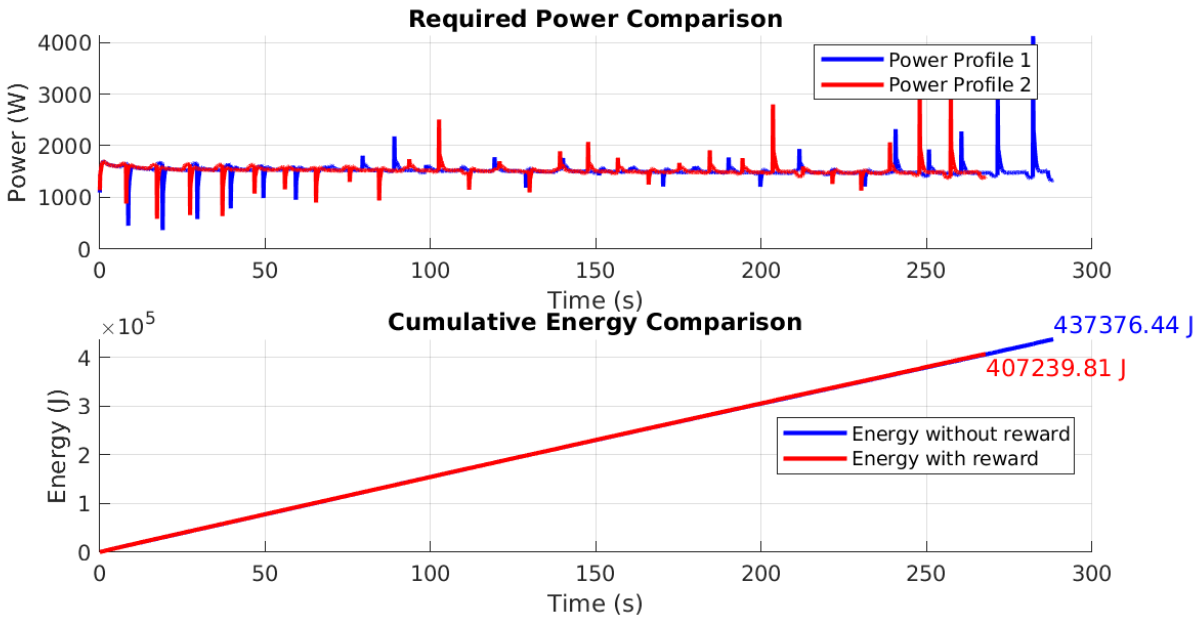

Fig. 5 Power and cumulative energy comparison of two flight missions with and without energy-related reward function

Once these trajectories are generated, we proceed to the lower layer of the proposed framework to perform prognostics and mission risk assessment. We generated 500 Monte Carlo simulations to assess the feasibility of each mission. Additionally, to determine the probability of mission success or failure, we established a threshold State of Charge (SoC_{th}) value of 30% at the end of the flight. Figure 3 shows the SoC predictions for the six flight missions mentioned above. Finally, to decide whether to conduct the mission or not, we used Equation 11 along with the constructed SoC PDF, SoC_{th}, and a probability threshold $P_{\text{threshold}}$ value of 95%. As mentioned in Algorithm 1, this $P_{\text{threshold}}$ value is used to determine the execution of the mission. Specifically, in our case, if the probability of an aircraft arriving at its destination with a SoC value of 30% is above 95%, then our framework will decide to execute the mission. Accordingly, the final decisions for the mission shown in Figure 4 are given in Table 2.

Table 2 Mission Success Probabilities and Decisions

Mission ID	Success Probability	Decision
1	0.97	Cleared for Flight
2	0.00	Hold
3	1.00	Cleared for Flight
4	0.10	Hold
5	1.00	Cleared for Flight
6	1.00	Cleared for Flight

V. Conclusion

This work addresses the problem of developing a decision-making framework that performs pre-departure flight planning and flight mission risk assessment for UAM and UAS applications. The framework adopts a two-layer approach, where the upper layer is responsible for strategic de-confliction, and the lower layer performs prognostics and decision-making regarding the execution of the mission. We showcased the performance of the framework in a UAS scenario designed for package delivery application in the University Park area of the Dallas-Fort Worth metropolitan region. The results indicate the framework's potential to enhance safety and energy efficiency in UAM and UAS operations.

Acknowledgments

This project is supported by NASA Grant 80NSSC21M0087 under the NASA System-Wide Safety (SWS) program.

References

[1] Patterson, M. D., Antcliff, K. R., and Kohlman, L. W., "A proposed approach to studying urban air mobility missions including an initial exploration of mission requirements," *Annual Forum and Technology Display*, NASA NF1676L-28586, May 2018.

[2] Goodrich, K. H., and Theodore, C. R., "Description of the NASA urban air mobility maturity level (UML) scale," *AIAA Scitech 2021 forum*, 2021, p. 1627. https://doi.org/10.2514/6.2021-1627.

[3] Bosson, C., and Lauderdale, T. A., "Simulation evaluations of an autonomous urban air mobility network management and separation service," *2018 Aviation Technology, Integration, and Operations Conference*, 2018, p. 3365. https://doi.org/10.2514/6.2018-3365.

[4] Hoekstra, J. M., van Gent, R. N., and Ruigrok, R. C., "Designing for safety: the 'free flight'air traffic management concept," *Reliability Engineering & System Safety*, Vol. 75, No. 2, 2002, pp. 215–232. https://doi.org/10.1016/S0951-8320(01)00096-5.

[5] Valenti Clari, M., Ruigrok, R., and Hoekstra, J., "Cost-benefit study of free flight with airborne separation assurance," *AIAA Guidance, Navigation, and Control Conference and Exhibit*, 2001, p. 4361. https://doi.org/10.2514/6.2000-4361.

[6] Krozel, J., and Peters, M., "Conflict detection and resolution for free flight," *Air Traffic Control Quarterly*, Vol. 5, No. 3, 1997, pp. 181–212. https://doi.org/10.2514/atcq.5.3.181.

[7] Taye, A. G., Bertram, J., Fan, C., and Wei, P., "Reachability based Online Safety Verification for High-Density Urban Air Mobility Trajectory Planning," *AIAA AVIATION 2022 Forum*, 2022, p. 3542. https://doi.org/10.2514/6.2022-3542.

[8] Paielli, R. A., and Erzberger, H., "Conflict probability estimation for free flight," *Journal of Guidance, Control, and Dynamics*, Vol. 20, No. 3, 1997, pp. 588–596. https://doi.org/10.2514/2.4081.

[9] Bowers, K. L., "Determining the feasibility of a Flight Profile in a Free Flight Environment," *15th DASC. AIAA/IEEE Digital Avionics Systems Conference*, IEEE, 1996, pp. 81–86. https://doi.org/10.1109/DASC.1996.559139.

[10] Wing, D. J., Ballin, M. G., and Krishnamurthy, K., "Pilot in command: A feasibility assessment of autonomous flight management operations," *24th International Congress of the Aeronautical Sciences (ICAS 2004)*, 2004.

[11] Corbetta, M., and Kulkarni, C. S., "An approach for uncertainty quantification and management of unmanned aerial vehicle health," *Annual PHM Society Conference*, 2019. https://doi.org/10.36001/phmconf.2019.v11i1.847.

[12] Quinones-Grueiro, M., Biswas, G., Ahmed, I., Darrah, T., and Kulkarni, C., "Online decision making and path planning framework for safe operation of unmanned aerial vehicles in urban scenarios," *International Journal of Prognostics and Health Management*, Vol. 12, No. 3, 2021. https://doi.org/10.36001/ijphm.2021.v12i3.2953.

[13] Pradeep, P., and Wei, P., "Energy-efficient arrival with rta constraint for multirotor evtol in urban air mobility," *Journal of Aerospace Information Systems*, Vol. 16, No. 7, 2019, pp. 263–277. https://doi.org/10.2514/1.I010710.

[14] Pradeep, P., Lauderdale, T. A., Chatterji, G. B., Sheth, K., Lai, C. F., Sridhar, B., Edholm, K.-M., and Erzberger, H., "Wind-optimal trajectories for multirotor eVTOL aircraft on UAM missions," *AIAA AVIATION 2020 Forum*, 2020, p. 3271. https://doi.org/10.2514/6.2020-3271.

[15] Schumann, J., Kulkarni, C., Lowry, M., Bajwa, A., Teubert, C., and Watkins, J., "Prognostics for Autonomous Electric-Propulsion Aircraft," *International Journal of Prognostics And Health Management*, Vol. 12, No. 3, 2021. https://doi.org/10.36001/ijphm.2021.v12i3.2940.

[16] Taye, A., Thompson, E. L., Wei, P., Bonin, T., and Jones, J. C., "Probabilistic Evaluation for Flight Mission Feasibility of a Small Octocopter in the Presence of Wind," *AIAA AVIATION 2023 Forum*, 2023, p. 3964.

[17] Taye, A., Valenti, R., Rajhans, A., Mavrommati, A., Mosterman, P. J., and Wei, P., "Safe and Scalable Real-Time Trajectory Planning Framework for Urban Air Mobility," *arXiv preprint arXiv:2306.11647*, 2023.

[18] Corbetta, M., Banerjee, P., Okolo, W., Gorospe, G., and Luchinsky, D. G., "Real-time uav trajectory prediction for safety monitoring in low-altitude airspace," *AIAA AVIATION 2019 forum*, 2019, p. 3514. https://doi.org/10.2514/6.2019-3514.

[19] Marshall, J. A., Sun, W., and L'Afflitto, A., "A survey of guidance, navigation, and control systems for autonomous multi-rotor small unmanned aerial systems," *Annual Reviews in control*, Vol. 52, 2021, pp. 390–427. https://doi.org/10.1016/j.arcontrol.2021.10.013.

[20] Daigle, M., and Kulkarni, C. S., "Electrochemistry-based battery modeling for prognostics," *Annual Conference of the PHM Society*, Vol. 5, 2013. https://doi.org/10.36001/phmconf.2013.v5i1.2252.

[21] Teubert, C., Jarvis, K., Corbetta, M., Kulkarni, C., and Daigle, M., "ProgPy: Python Packages for Prognostics and Health Management of Engineering Systems," *Journal of Open Source Software*, Vol. 8, No. 87, 2023, p. 5099.

[22] Wan, E. A., and Van Der Merwe, R., "The unscented Kalman filter," *Kalman filtering and neural networks*, 2001, pp. 221–280. https://doi.org/10.1002/0471221546.ch7.

[23] Ekwaro-Osire, S., Gonçalves, A. C., Alemayehu, F. M., et al., *Probabilistic prognostics and health management of energy systems*, Springer, 2017. https://doi.org/10.1007/978-3-319-55852-3_1.

[24] Ahmed, I., Quinones-Grueiro, M., and Biswas, G., "A high-fidelity simulation test-bed for fault-tolerant octo-rotor control using reinforcement learning," *2022 IEEE/AIAA 41st Digital Avionics Systems Conference (DASC)*, IEEE, 2022, pp. 1–10.